Nanoscale

COMMUNICATION

View Article Online
View Journal | View Issue

Hematite concave nanocubes and their superior catalytic activity for low temperature CO oxidation†

Cite this: *Nanoscale*, 2014, **6**, 7199

Received 28th January 2014
Accepted 14th April 2014

DOI: 10.1039/c4nr00552j

www.rsc.org/nanoscale

Hanfeng Liang,[a] Xinde Jiang,[b] Zhengbing Qi,[a] Wei Chen,[a] Zhengtao Wu,[a] Binbin Xu,[ac] Zhoucheng Wang,*[a] Jinxiao Mi[c] and Qingbiao Li[a]

Hematite (α-Fe_2O_3) concave nanocubes bound by high-index {13$\bar{4}$4} and {12$\bar{3}$8} facets were synthesized and their catalytic activity for CO oxidation were also investigated.

Nanocrystals (NCs) enclosed by high energy facets have attracted much attention due to their high activities in many processes such as heterogeneous catalysis, energy conversion, and gas sensing.[1] However, the surfaces with high energy are thermodynamically unstable and usually disappear during the growth of NCs.[1b] Therefore, it is a big challenge to synthesize NCs with high-index facets. Thanks to the efforts from many research groups, a large number of NCs, such as Au, Pt, TiO_2, Cu_2O, SnO_2 and α-Fe_2O_3, with high-index facets exposed have been prepared.[2] In most cases, these NCs are polyhedra encased by convex surfaces. Despite great successes having been achieved in the synthesis of NCs with convex surfaces, the synthesis of NCs with concave surfaces, however, is still in an embryonic stage which may draw more attention since the concave structures are expected to show unexplored or substantially enhanced properties relative to their convex counterparts.[1c] Many groups have demonstrated the synthesis of concave noble metals, including Au, Ag, Pd, Pt, Rh, as well as their bimetallic combinations by various methods such as facet-selective capping, kinetically controlled overgrowth and site-specific etching.[3] In contrast, the synthesis of concave metal oxides is considerably difficult due to their more complicated structures and stronger metal–oxygen bonds. And there has not been any report on concave metal oxides except for Cu_2O.[2e] However it should be pointed out that Cu_2O, as well as noble metals, are all in cubic systems, and the fabrication of other concave metal oxides that do not crystallize in cubic crystalline systems is still limited.

Hematite (α-Fe_2O_3), as an important n-type semiconductor with a band gap of 2.2 eV, has been widely used in water splitting, catalysis, sensors and lithium-ion batteries.[4] To date, various well-defined α-Fe_2O_3 NCs, such as spindles, plates, and well-shaped polyhedra, have been synthesized, expecting to enhance their performance in many applications.[5] For example, Sun and co-workers demonstrated the synthesis of dodecahedral α-Fe_2O_3 particles with {10$\bar{1}$1} and {11$\bar{2}$1} planes exposed by a fluoride anion-assisted hydrothermal method.[2h] Despite these successes, the synthesis of α-Fe_2O_3 NCs with high-index facets exposed still remains a big challenge. Moreover, as a limitation, these polyhedra that were reported in previous studies are all encased by convex surfaces. Here, we report a simple copper ion-assisted hydrothermal route based on kinetically controlled overgrowth to the synthesis of α-Fe_2O_3 concave 'nanocubes' bound by high-index {13$\bar{4}$4} and {12$\bar{3}$8} facets. Different from noble metals and some metal oxides (*e.g.* Cu_2O) with cubic crystalline systems, α-Fe_2O_3 belongs to the trigonal system, thus the exposed high-index facets of concave nanocubes are very special. When evaluated as a catalyst for CO oxidation, the obtained α-Fe_2O_3 concave nanocubes exhibited superior catalytic activity and high stability.

In a typical synthesis of concave nanocubes, a mixture of $Fe(NO_3)_3$, cupric acetate ($CuOAc_2$), and ammonium hydroxide was kept at 140 °C under hydrothermal conditions for 16 h. The structure of the as-prepared α-Fe_2O_3 concave nanocubes was characterized using X-ray diffraction (XRD, Fig. S1a, ESI†). All the diffraction peaks are in good agreement with those of hematite (JCPDS no. 33-0664), which suggests that the obtained concave nanocubes have a trigonal iron oxide structure ($R\bar{3}c$) with high purity. Although the diffraction peaks do not show significant shift, the result from XRD Rietveld refinement still shows that the obtained cell parameters are sensibly different from those in JCPDS 33-0664, suggesting Cu^{2+} ions may be doped into α-Fe_2O_3 crystals (Fig. S1b, ESI†). The existence of Cu^{2+} ions is further confirmed by the X-ray photoelectron spectroscopy (XPS, Fig. S1e, ESI†) and energy-dispersive X-ray spectrometry (EDX, Fig. S8, ESI†) analyses. Fig. 1a shows a

[a]*College of Chemistry and Chemical Engineering, Xiamen University, Xiamen 361005, China. E-mail: zcwang@xmu.edu.cn; Fax: +86 592 2180738; Tel: +86 592 2180738*

[b]*College of Science, Nanchang Institute of Technology, Nanchang 330099, China*

[c]*College of Materials, Xiamen University, Xiamen 361005, China*

† Electronic supplementary information (ESI) available. See DOI: 10.1039/c4nr00552j

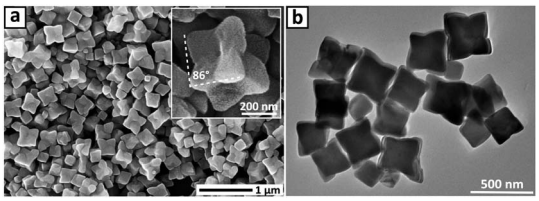

Fig. 1 (a) Typical large-area and high-magnification (inset) SEM images of α-Fe_2O_3 concave nanocubes. (b) TEM image of α-Fe_2O_3 concave nanocubes.

typical scanning electron microscopy (SEM) image of the obtained product, indicating the presence of well-distributed NCs with an edge length (defined as the distance between adjacent corners) of *ca.* 280–350 nm. Close observation of an individual concave nanocube (the inset of Fig. 1a) clearly reveals that each face of the nanocube (in fact the shape is pseudocubic since one of dihedral angles between adjacent facets is 86°) was excavated by a curved cavity in the centre. Transmission electron microscopy (TEM) characterization (Fig. 1b) further confirms the formation of concave structures as the NCs exhibited a darker contrast in the centre than at the edges. Statistical analysis of 200 particles based on TEM indicates that the yield of the concave nanocubes is about 86%.

Fig. 2a shows the TEM images obtained from a single concave nanocube at different tilting angles. Deep dents on the surfaces of the nanocubes can be clearly observed, supporting the formation of a concave rather than a flat surface on each lateral face. The images observed are also consistent with the proposed geometric models (Fig. 2b). Fig. 2c shows a high-resolution TEM image of an individual concave nanocube viewed along the $[2\bar{2}01]$ direction, as confirmed by the corresponding selected area electron diffraction (SAED) pattern

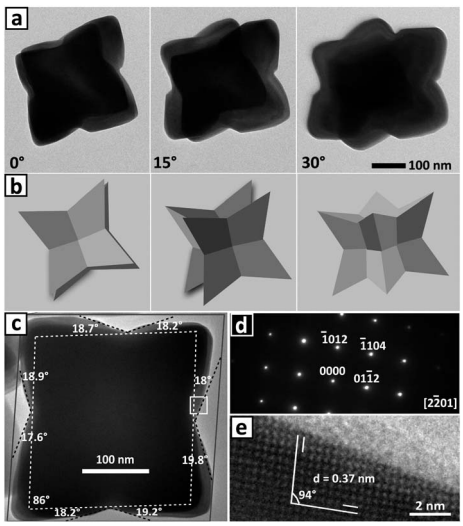

Fig. 2 (a) TEM images recorded at different tilting angles and (b) the corresponding geometric models of a hematite concave nanocube. (c) TEM image of an individual hematite concave nanocube, (d) corresponding SAED pattern and (e) HRTEM image of the region indicated by the square in (c).

(Fig. 2d). It can be seen that eight lateral facets of the concave nanocube were projected edge-on. For rhombohedral hematite structures, if a crystal facet of the concave nanocube is already given, then the Miller indices of its adjacent crystal facets can be derived from the projection angles along a selected crystallographic axis. By comparing the measured and calculated values of projected angles (Fig. S2 and S3, ESI†), the eight edge-on facets can be indexed as $\{13\bar{4}4\}$ and $\{12\bar{3}8\}$ planes. The high-resolution TEM (HRTEM) image of an edge of an individual concave nanocube is shown in Fig. 2e. The lattice spacing was measured to be 0.37 nm, which is in agreement with the $\{01\bar{1}2\}$ lattice spacing of rhombohedral hematite, indicating the single-crystalline nature of the as-obtained product.

Using additives is very common and effective to control the shape and size of nanostructures. In previous studies, metal ions were seldom used as additives in the synthesis of metal oxides since the introduction of metal ions might lead to the formation of undesired metal oxides or hydroxides.[6] In our system, $NH_3 \cdot H_2O$ was used instead of NaOH to offer an alkali environment, and more importantly, to avoid the formation of CuO. As we know, Cu^{2+} ions can react easily with $NH_3 \cdot H_2O$ to form $[Cu \cdot (NH_3)_4]^{2+}$ complexes, which can resolve into the solution. Thus, at a high concentration of $NH_3 \cdot H_2O$ (*e.g.* 3 mL), only α-Fe_2O_3 NCs can be obtained although there is $CuOAc_2$ in the system. In contrast, CuO can also be obtained if the concentration of $NH_3 \cdot H_2O$ is relatively low (*e.g.* 0.5 mL, Fig. S4, ESI†). Besides $NH_3 \cdot H_2O$, $CuOAc_2$ is also found to be essential for the formation of α-Fe_2O_3 concave nanocubes. The reaction in the absence of $CuOAc_2$ yields α-Fe_2O_3 NCs with mixed morphologies (*e.g.* hexagonal bipyramids and rods, Fig. S5a, ESI†). To find out the role that $CuOAc_2$ played, we conducted a set of experiments using the standard procedure, except that different copper salts were used. The result shows that the concave nanocubes can also be obtained in the presence of other copper salts such as $CuSO_4$, $Cu(NO_3)_2$ and $CuCl_2$ (Fig. S5, ESI†), suggesting that the existence of Cu^{2+} ions are responsible for the formation of α-Fe_2O_3 concave nanocubes. To gain insight into the details of morphological evolution during the growth of the α-Fe_2O_3 concave nanocubes, time-dependent experiments were carried out (Fig. 3). In the first 6 h, the transformation of dense aggregates of primary nanoparticles into nanocubes can be attributed to the dissolution–recrystallization process and continuous growth *via* Ostwald ripening. The chemical reactions involved in this system can be formulated as follows:

$$NH_3 \cdot H_2O \leftrightarrow NH_4^+ + OH^- \quad (1)$$

$$Fe^{3+} + 3OH^- \rightarrow Fe(OH)_3 \quad (2)$$

$$2Fe(OH)_3 \rightarrow Fe_2O_3 + 3H_2O \quad (3)$$

$$Cu^{2+} + 2OH^- \rightarrow Cu(OH)_2 \quad (4)$$

$$Cu(OH)_2 \rightarrow CuO + H_2O \quad (5)$$

$$Cu(OH)_2 + 4NH_3 \rightarrow [Cu(NH_3)_4]^{2+} + 2OH^- \quad (6)$$

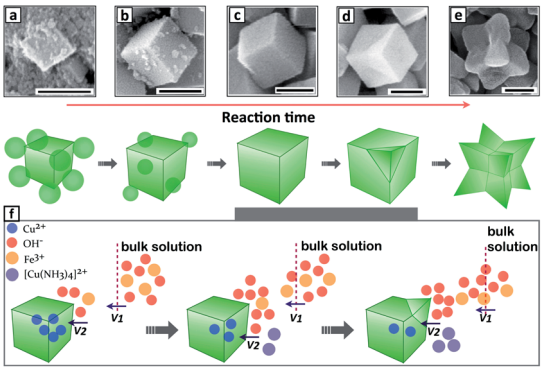

Fig. 3 SEM images of the nanocrystals collected at different reaction times: (a) 1 h, (b) 2 h, (c) 6 h, (d) 10 h, and (e) 16 h. Scale bars: 200 nm. Low magnification SEM images and XRD patterns of the nanocrystals collected at 1, 2, 6, and 10 h are shown in Fig. S6 in the ESI†. (f) Schematic diagram of the kinetically controlled overgrowth (when V_2 is much larger than V_1) of concave nanocubes evolved from pseudo-nanocubes.

At the initial reaction stage, the Fe^{3+} and Cu^{2+} ions may form $Fe(OH)_3$ and $Cu(OH)_2$ under alkaline conditions, respectively. As time goes on, $Fe(OH)_3$ decomposes into α-Fe_2O_3. While instead of decomposing into CuO, $Cu(OH)_2$ reacts with excess $NH_3 \cdot H_2O$ to form $[Cu(NH_3)_4]^{2+}$ complexes, which can dissolve into the solution and may adsorb onto the specific surface of α-Fe_2O_3 NCs, leading to the formation of nanocubes bound by six $\{01\bar{1}2\}$ facets (Fig. S7, ESI†). The nanocubes subsequently grow at the expense of nanoparticles until all the particles are consumed. With the increase of reaction time, the size of nanocubes increases as observed, *e.g.* 120–140 nm (1 h), 130–160 nm (2 h), and 200–220 nm (6 h), respectively (Fig. 3a–c). The following growth process from 10 to 16 h is quite interesting. In previous reports, most of the concave nanocubes (for those crystallize in cubic crystal systems, such as noble metals) were synthesized by facet-selective capping or kinetic controlled overgrowth.[3a–e] The basic principle is to retard the growth of {100} facets and/or promote the growth of {111} facets of a cubic seed. In our case, the growth of concave nanocubes is more complicated while it can still be considered as a kinetically controlled process. It has been demonstrated by Chernov that during a kinetic growth process, two factors, namely the diffusion rate of precursor (V_1) from solution to the surface and the growth rate (V_2) at which atoms were generated and added to the surface of a growing seed, played a critical role in determining the growth habit of a seed.[7] When V_1 is much larger than V_2, the fast diffusion ensures the concentration of the precursor identical in close proximity to the surface of seeds and the bulk solution. The atoms would be added on different sites of seeds with equal probability. In the initial 6 h, the concentration of the precursor is relatively sufficient, thus Ostwald ripening rather than preferential overgrowth occurred under this condition (Fig. 3a–c). On the other hand, when V_1 is much smaller than V_2, there will be a gradient for the precursor concentration from high to low corresponding to the area from bulk solution to the surface of the seeds. Under this condition, the atom generated on the surface of a nanocube would be preferentially added to the site with the highest reactivity owing to an insufficient supply of atoms.[3e] And for a nanocube, the eight corners have the highest reactivity. That means concave nanocubes can be obtained from the cubic seeds by kinetically controlled overgrowth (when V_1 is much smaller than V_2). Herein, the dissolution of Cu^{2+} ions and subsequent formation of the $[Cu(NH_3)_4]^{2+}$ complexes play a key role in the kinetic overgrowth process. To confirm the dissolution of Cu^{2+} ions, EDX line scan of the products was carried out (Fig. S8, ESI†). The Cu–Fe elemental ratio of the product obtained after 10 h is obviously higher than that of the product obtained after 16 h, suggesting that the Cu^{2+} ions dissolve into the bulk solution during the reaction. Therefore, it is reasonable that the Cu^{2+} ions in the interior of α-Fe_2O_3 NCs would dissolve into the solution in the form of the $[Cu(NH_3)_4]^{2+}$ complexes and consequently lead to the generation of OH^- around the surface [see eqn (4)–(6) and Fig. 3f]. Apparently, the Fe^{3+} ions are insufficient at this time compared with OH^-. Thus, the diffusion rate (V_1) of Fe^{3+} ions plays a critical role in the seed growth. The Fe^{3+} ions in close proximity to the surface of the nanocubes will react rapidly with much excess OH^- anions. Thus V_2 is much larger than V_1. With insufficient supply of Fe^{3+} ions, the Fe^{3+} ions would prefer to react with OH^- anions on the sites with the highest reactivity, namely the corners. It can be seen clearly that a triangular pyramid is first developed from one corner of a nanocube (Fig. 3d). Then the vertexes and edges of triangular pyramids grow along the edges and facets of a nanocube, respectively, leading to the formation of a concave nanocube. It should be pointed out that hematite belongs to the trigonal system, therefore, its growth habit is supposed to be different from NCs that crystallize in cubic crystalline systems. For concave cubic structural NCs (*e.g.* Au, Ag, Pd) that crystallize in cubic crystalline systems, the growth rates along the ⟨111⟩ directions are theoretically equivalent to each other during the evolution from cubic seeds to concave nanocubes. While in our case, the triangular pyramid developed along the longest diagonal axis (*c*-axis) of the nanocube would grow much faster as a result of the preferential growth in this direction (Fig. S9, ESI†). This is the characteristic of rhombohedral crystals and is totally different from cubic crystals. This preferential growth can be further confirmed by a close TEM observation of the concave nanocubes, which clearly shows that one of the eight corners of the concave nanocubes is obviously much bigger than the others (Fig. S10, ESI†).

The obtained α-Fe_2O_3 concave nanocubes were then evaluated as catalysts for CO oxidation. Porous α-Fe_2O_3 nanorods with a length of *ca.* 300 nm and a diameter of *ca.* 50 nm were synthesized and their catalytic activities were also investigated for comparison (Fig. S11, ESI†). Fig. 4 shows the conversion of CO oxidation over the two catalysts as a function of reaction temperature. Generally, catalysts with a large surface area often exhibit high catalytic activities, while many studies have shown that the crystal planes might play an even more important role in determining the catalytic activities of the catalysts.[8] For example, Tao *et al.* found that the Fe_2O_3 nanocubes bound by $\{01\bar{1}2\}$ facets exhibited a higher catalytic activity towards CO

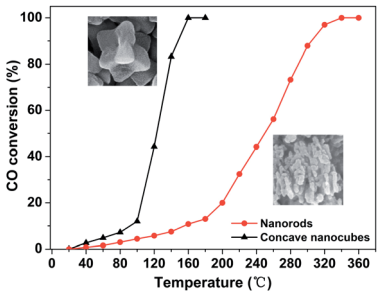

Fig. 4 Catalytic activities of α-Fe_2O_3 concave nanocubes and nanorods for CO oxidation. Feed gas containing 1 vol% CO, 1 vol% O_2 and balance N_2 is at a total flow rate of 60 mL min^{-1}, corresponding to a GHSV of 36 000 mL g^{-1} h^{-1}.

oxidation than nanotubes with {01$\bar{1}$0} facets exposed although their surface area was much smaller than that of nanotubes (0.384 and 13.7 m^2 g^{-1} for nanocubes and nanotubes, respectively).[8c] Similarly, in our case, despite the smaller BET surface area and pore-free structure (13.5 m^2 g^{-1} for concave nanocubes and 39.3 m^2 g^{-1} for porous nanorods, Table S1, ESI†), the catalytic activity of α-Fe_2O_3 concave nanocubes is remarkably higher than that of α-Fe_2O_3 nanorods. The light-off temperature $T_{50\%}$ (the temperature at which the conversion of CO reaches 50%) of concave nanocubes is as low as 124 °C, and 100% CO conversion is achieved at 160 °C. In contrast, the CO conversion over nanorods at 160 °C is only 10.8%. The specific rates of CO oxidation over the two catalysts also provide clear evidence that the concave nanocubes are more active than nanorods (Fig. S12a, ESI†). For example, the reaction rate of CO oxidation on the concave nanocubes is 1.98×10^{-6} mol CO per g per s at 120 °C, which is almost 8 times as large as that of porous nanorods (0.26×10^{-6} mol CO per g per s, Table S2, ESI†). However, the estimated apparent activation energies (E_a) over the two catalysts are close to each other (21.1 and 24.9 kJ mol^{-1} for concave nanocubes and nanorods respectively, Fig. S12b, ESI†), which implies that the morphology affects the reaction rate significantly but has little influence on the reaction pathway.[9] It is worth mentioning that the reaction temperature of 160 °C for 100% CO conversion over the as-prepared α-Fe_2O_3 concave nanocubes is much lower than those previously reported for iron oxides, other metal oxides (or their composites) and even some noble metal/metal oxide composites (Table S3, ESI†). The α-Fe_2O_3 concave nanocubes also show high stability. No deactivation occurs when the catalytic reaction is performed at 160 °C for 72 h (Fig. S13, ESI†). The enhanced activity of the as-obtained α-Fe_2O_3 concave nanocubes for CO oxidation could be attributed to their high-index facets.

It is noted that in our case, the α-Fe_2O_3 concave nanocubes were doped with Cu^{2+}. The existence of Cu^{2+} ions is confirmed by the XPS and EDX results. We further carried out the inductively coupled plasma mass spectrometry (ICP-MS) measurement. And the result shows that the amount of Cu is about 2.5 wt%. Doping has been regarded as an efficient way to enhance the catalytic performance of a catalyst because the addition of dopants can greatly increase the number of oxygen vacancies and improve the thermal stability.[10] And the oxygen vacancies, even in small amounts, could benefit the catalytic reaction since they provide sites for oxygen activation to form superoxide species.[10b] Many studies have suggested that the doped catalysts generally exhibited better catalytic activities than the pristine catalysts. For example, Luo *et al.* found that Pr- and Cu-doped CeO_2 catalysts showed enhanced activities for CO oxidation compared with bare CeO_2.[10b] In this work, the copper doping may also lead to the formation of oxygen vacancies of the catalyst, resulting in an enhanced activity for the CO oxidation.

In summary, α-Fe_2O_3 concave nanocubes enclosed by high-index {13$\bar{4}$4} and {12$\bar{3}$8} facets were synthesized *via* a facile hydrothermal route based on kinetically controlled growth. The as-obtained concave α-Fe_2O_3 nanocubes exhibited superior catalytic activity and high stability for CO oxidation. This work provides a new method to fabricate low-cost and highly active α-Fe_2O_3 concave nanocubes, which can find promising applications in catalysis, water splitting and solar cells owing to their unique structure and properties.

Acknowledgements

The authors thank the State Key Development Program for Basic Research of China (Grant no. 2007CB935603) and the National Science Foundation of China (Grant no. 51372212) for financial support.

Notes and references

1 (*a*) Z. Y. Zhou, N. Tian, J. T. Li, I. Broadwell and S. G. Sun, *Chem. Soc. Rev.*, 2011, **40**, 4167; (*b*) N. Tian, Z. Y. Zhou and S. G. Sun, *J. Phys. Chem. C*, 2008, **112**, 19801; (*c*) H. Zhang, M. Jin and Y. Xia, *Angew. Chem., Int. Ed.*, 2012, **51**, 7656.

2 (*a*) J. W. Hong, S. U. Lee, Y. W. Lee and S. W. Han, *J. Am. Chem. Soc.*, 2012, **134**, 4565; (*b*) N. Tian, Z. Y. Zhou, S. G. Sun, Y. Ding and Z. L. Wang, *Science*, 2007, **316**, 732; (*c*) N. Tian, Z. Y. Zhou, N. F. Yu, L. Y. Wang and S. G. Sun, *J. Am. Chem. Soc.*, 2010, **132**, 7580; (*d*) S. Liu, J. Yu and M. Jaroniec, *Chem. Mater.*, 2011, **23**, 4085; (*e*) M. J. Siegfried and K. S. Choi, *Angew. Chem., Int. Ed.*, 2005, **44**, 3218; (*f*) X. Han, L. Li and C. Wang, *Chem.–Asian J.*, 2012, **7**, 1572; (*g*) X. Wang, X. Han, S. Xie, Q. Kuang, Y. Jiang, S. Zhang, X. Mu, G. Chen, Z. Xie and L. Zheng, *Chem.–Eur. J.*, 2012, **18**, 2283; (*h*) B. Lv, Z. Liu, H. Tian, Y. Xu, D. Wu and Y. Sun, *Adv. Funct. Mater.*, 2010, **20**, 3987; (*i*) Z. Liu, B. Lv, D. Wu, Y. Sun and Y. Xu, *Eur. J. Inorg. Chem.*, 2012, 4076; (*j*) Y. Yang, H. Ma, J. Zhuang and X. Wang, *Inorg. Chem.*, 2011, **50**, 10143; (*k*) R. D. Rodriguez, D. Demaille, E. Lacaze, J. Jupille, C. Chaneac and J. P. Jolivet, *J. Phys. Chem. C*, 2007, **111**, 16866.

3 (*a*) D. Kim, T. Yu, E. Cho, Y. Ma, O. Park and Y. Xia, *Angew. Chem., Int. Ed.*, 2011, **50**, 6328; (*b*) X. Xia, J. Zeng, B. Mcdearmon, Y. Zheng, Q. Li and Y. Xia, *Angew. Chem., Int. Ed.*, 2011, **50**, 12542; (*c*) X. Q. Huang, S. H. Tang, H. H. Zhang, Z. Y. Zhou and N. F. Zheng, *J. Am. Chem. Soc.*, 2009, **131**, 13916; (*d*) T. Herricks, J. Y. Chen and Y. Xia, *Nano Lett.*, 2004, **4**, 2367; (*e*) M. Jin, H. Zhang, Z. Xie and

Y. Xia, *Angew. Chem., Int. Ed.*, 2011, **50**, 7850; (*f*) H. Zhang, W. Y. Li, M. S. Jin, J. E. Zeng, T. K. Yu, D. R. Yang and Y. Xia, *Nano Lett.*, 2011, **11**, 898; (*g*) Y. J. Deng, N. Tian, Z. Y. Zhou, R. Huang, Z. L. Liu, J. Xiao and S. G. Sun, *Chem. Sci.*, 2012, **3**, 1157.

4 (*a*) I. Cesar, A. Kay, J. A. G. Martinez and M. Grätzel, *J. Am. Chem. Soc.*, 2006, **128**, 4582; (*b*) X. Zhou, J. Lan, G. Liu, K. Deng, Y. Yang, G. Nie, J. Yu and L. Zhi, *Angew. Chem.*, 2012, **124**, 182; (*c*) J. Chen, L. Xu, W. Li and X. Gou, *Adv. Mater.*, 2005, **17**, 582; (*d*) B. Koo, H. Xiong, M. D. Slater, V. B. Prakapenka, M. Balasubramanian, P. Podsiadlo, C. S. Johnson, T. Rajh and E. V. Shevchenko, *Nano Lett.*, 2012, **12**, 2429.

5 (*a*) H. Liang, W. Chen, X. Jiang, X. Xu, B. Xu and Z. Wang, *J. Mater. Chem. A*, 2014, **2**, 4340; (*b*) X. Li, W. Wei, S. Wang, L. Kuai and B. Geng, *Nanoscale*, 2011, **3**, 718; (*c*) H. Liang, X. Xu, W. Chen, B. Xu and Z. Wang, *CrystEngComm*, 2014, **16**, 959; (*d*) H. Jiang, B. Geng, L. Kuai and S. Wang, *Chem. Commun.*, 2011, **47**, 2447; (*e*) H. Liang, B. Xu and Z. Wang, *Mater. Chem. Phys.*, 2013, **141**, 727; (*f*) H. Liang and Z. Wang, *Mater. Lett.*, 2013, **96**, 12.

6 (*a*) R. M. Cornell and R. Giovanoli, *J. Chem. Soc., Chem. Commun.*, 1987, 413; (*b*) M. H. Yang, P. C. Chen, M. C. Tsai, T. T. Chen, I. C. Chang, H. T. Chiu and C. Y. Lee, *CrystEngComm*, 2013, **15**, 2966.

7 A. Chernov, *Sov. Phys. Crystallogr.*, 1972, **16**, 734.

8 (*a*) K. Zhou, X. Wang, X. Sun, Q. Peng and Y. Li, *J. Catal.*, 2005, **229**, 206; (*b*) Tana, M. Zhang, J. Li, H. Li, Y. Li and W. Shen, *Catal. Today*, 2009, **148**, 179; (*c*) Q. X. Gao, X. F. Wang, J. L. Di, X. C. Wu and Y. R. Tao, *Catal. Sci. Technol.*, 2011, **1**, 574.

9 X. Xie and W. Shen, *Nanoscale*, 2009, **1**, 50.

10 (*a*) S. Carrettin, Y. Hao, V. Aguilar-Guerrero, B. C. Gates, S. Trasobares, J. J. Calvino and A. Corma, *Chem.–Eur. J.*, 2007, **13**, 7771; (*b*) Z. Y. Pu, X. S. Liu, A. P. Jia, Y. L. Xie, J. Q. Lu and M. F. Luo, *J. Phys. Chem. C*, 2008, **112**, 15045; (*c*) J. B. Wang, D. H. Tsai and T. J. Huang, *J. Catal.*, 2002, **208**, 370.